Linear polarization of the characteristic x-ray lines following inner-shell photoionization of tungsten

T. Kämpfer,[1,2] I. Uschmann,[1,2] Z. W. Wu,[2,3] A. Surzhykov,[2] S. Fritzsche,[2,4] E. Förster,[1,2] and G. G. Paulus[1,2]

[1]*Institut für Optik und Quantenelektronik, Friedrich-Schiller-Universität Jena, Max-Wien-Platz 1, D-07743 Jena, Germany*

[2]*Helmholtz-Institut Jena, Fröbelstieg 3, D-07743 Jena, Germany*

[3]*Key Laboratory of Atomic and Molecular Physics & Functional Materials of Gansu Province, College of Physics and Electronic Engineering, Northwest Normal University, Lanzhou 730070, People's Republic of China*

[4]*Theoretisch-Physikalisches Institut, Friedrich-Schiller-Universität Jena, Max-Wien-Platz 1, D-07743 Jena, Germany*

(Received 18 December 2015; published 9 March 2016)

The linear polarization of the characteristic lines $L\alpha_1$ ($3d_{5/2} \rightarrow 2p_{3/2}$) and $L\alpha_2$ ($3d_{3/2} \rightarrow 2p_{3/2}$), following inner-shell photoionization of neutral tungsten, is analyzed both experimentally and theoretically. In the experiment, a tungsten target is photoionized by the primary emission of an x-ray tube with incident photon energies in the range of 10.2–30 keV. The σ and π components of the emitted fluorescence are measured by using a spectropolarimeter, based on x-ray diffraction at Bragg angles close to 45°. The degree of linear polarization of the $L\alpha_1$ and $L\alpha_2$ lines is determined to be $+(1.6 \pm 0.5)\%$ and $-(7 \pm 2)\%$, respectively. In addition, this degree of polarization is calculated within the framework of the density-matrix theory as a function of the incident photon energy. These calculations are in good agreement with the experimental results and show only a weak dependence of the degree of polarization on the energy of the incident photoionizing photon.

DOI: 10.1103/PhysRevA.93.033409

I. INTRODUCTION

The inner-shell ionization of a neutral atom results in the production of an excited ionic state. The subsequent decay of this state may lead to the emission of x rays with a wavelength that is characteristic of the ionized atom. While the spectroscopic analysis of the characteristic x rays is widely explored in science and technology, less effort has been placed on the more subtle signatures of these ionization and decay processes, such as the linear polarization of the emitted photons.

The fact that the characteristic lines are possibly polarized was predicted theoretically for the first time by Mehlhorn [1]. In that work it was shown that the excitation of the atomic levels with a total angular momentum $J > 1/2$ by a particle beam induces a nonstatistical population of the magnetic substates. Such a nonstatistical population was referred to as the alignment. In a further theoretical work by Flügge *et al.* [2], such an alignment was predicted also for the ionization of atoms with unpolarized photons. Due to an alignment of these atomic states, the characteristic x-ray photons emitted from them are always anisotropic and polarized. In general, the angular distribution, as well as the degree of linear polarization of characteristic lines following photoionization, is related to a set of alignment parameters $\mathcal{A}_{kq}$ that depend not only on the shell structure of target atom but also on the energy and polarization of the incident light. The precise measurement of these polarization properties could therefore provide an effective tool to test different theoretical models used to describe the overall ionization and subsequent decay.

Since the early predictions in Ref. [1], many theoretical [3–7] and experimental (see [8–10] and references therein) studies have been performed to explore further the alignment and polarization phenomenon. In particular, the alignment of heavy ions after photoionization was discussed very controversially in the past (see Refs. [10–12] for further details). The alignment of the heavy ions is most generally studied by measuring the angular distribution of the characteristic lines. It turns from theoretical calculations, for example, for photoionization of Au and Pb atoms [4,10] with photon energies 1–10 keV above of the L_3 absorption edge, that the predicted anisotropies and degrees of linear polarization of the L lines (i.e., Ll, $L\alpha_{1,2}$, $L\beta$, ...) are typically quite small (a few percent). Experimentally, the measurement of the angular distribution is not straightforward, because usually corrections for the absorption of the incident beam and the emitted photons need to be applied. Those corrections, of course, introduce specific errors to the measurements. Moreover, it was shown by Yamaoka *et al.* [10] that the resolution of their solid-state detector limits the experimental errors for the angular distribution measurement to a few percent. In Refs. [12–14], however, small anisotropies close to the theoretical predictions have been measured with different instrumentation on synchrotron radiation sources.

In the present work we show that the alignment of the inner-shell ionized atoms can be studied with high accuracy by measuring the linear polarization with a well-characterized crystal-based x-ray polarimeter. With such a polarimeter we can not only distinguish relatively narrow fine-structure components but also study their linear polarization at the same time. Furthermore, as we measure the polarization of the fluorescence in just one selected spatial direction, no absorption corrections need to be applied to the data. We show that the experimental results for the photoionization of neutral tungsten by incident x-ray photons with energies in the range of 10.2–30 keV, emitted from an x-ray tube, are consistent with the theoretical predictions based on the density-matrix theory.

It is worth mentioning that this technique can be applied to almost any other atomic system or characteristic line in the hard x-ray range by selecting appropriate analyzer crystals and reflections. In particular, a transfer of this technique to modern synchrotron facilities will enable the study of these subtle effects to be more effective, such as the dependence on the photon energy or the polarization of ionizing radiation.

The paper is organized as follows. In Sec. II we present a brief description of the x-ray source, the polarimeter, and

 ©2016 American Physical Society

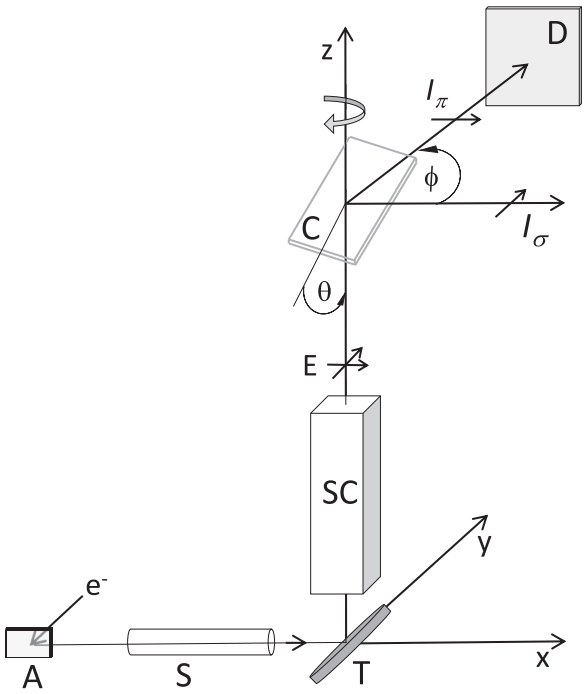

FIG. 1. Scheme of the experiment to measure the polarization of the $L\alpha_{1,2}$ lines following inner-shell photoionization of a tungsten target T. The entire polarimeter that consists of the Soller-collimator SC, the LiF analyzer crystal C, and the CCD detector D is mounted rotatable around the common z axis. (Here A denotes the molybdenum anode and S the circular aperture.) At the analyzer angles $\phi = 0°,90°$ and the Bragg angles θ close to 45°, the polarization components perpendicular I_σ and parallel I_π to the xz reaction plane are measured independently.

the parameters relevant to the experiment. In Sec. III we describe briefly the density-matrix theory that is used to analyze the linear polarization of x-ray fluorescence radiated from photoionized atoms. In Sec. IV the experimental results are discussed together with the theoretical predictions. We summarize in Sec. V.

II. EXPERIMENT

A sketch of the experiment is depicted in Fig. 1. It basically consists of two components, the x-ray light source for photoionization and the crystal-based x-ray polarimeter used to measure the polarization of the emitted fluorescence.

A. X-ray source

The primary radiation of an x-ray tube (30 kV and 40 mA) equipped with a molybdenum anode is collimated in the x direction by a circular aperture in order to photoionize a tungsten fluorescence target [15]. The photoionizing radiation is composed of the characteristic radiation of the anode material, Mo $K\alpha$ (17.5 keV) and Mo $K\beta$ (19.6 keV) for the most part, as well as the bremsstrahlung radiation with photon energies up to 30 keV at the cutoff. Therefore, the L_3 ($2p_{3/2}$) level of tungsten at 10.207 keV and the subshells L_2 ($2p_{1/2}$, 11.544 keV) and L_1 ($2s$, 12.100 keV) are photoionized simultaneously by various photon energies. By just observing the $L\alpha_{1,2}$ ($3d_{5/2},3d_{3/2} \rightarrow 2p_{3/2}$) fluorescence with the polarimeter, we choose the L_3 ($2p_{3/2}$) subshell as the one of interest. In order to quantify an average photon energy $\bar{E}$, capable of ionizing the L_3 subshell, we have measured the energy distribution $I_0(E)$ of the photons on the target by using a lithium fluoride crystal spectrometer. From this distribution, an average photon energy

$$\bar{E} = \frac{\int_{10.2\ \mathrm{keV}}^{30\ \mathrm{keV}} I_0(E) E\, dE}{\int_{10.2\ \mathrm{keV}}^{30\ \mathrm{keV}} I_0(E) dE} = 18.5\ \mathrm{keV} \qquad (1)$$

was estimated. The number of photons shined on the target in the energy range from 10.2 to 30 keV is on the order of 10^{11} per second.

B. Polarimeter

The aim of our spectropolarimeter is to measure the spectrum and the polarization of the specific x-ray lines that are emitted along the z axis, perpendicular to the ionizing light beam (chosen as the x direction). The xz plane is then called the reaction plane, with the y axis as surface normal. For the analysis of polarization, intensities of the x-ray lines with the electric-field vector perpendicular to and parallel to the reaction plane, I_σ and I_π, respectively, are measured independently. Our polarimeter basically consists of a Soller collimator, an analyzer crystal, and a detector and is mounted as a whole rotatable by the angle ϕ around the common z axis. The angle ϕ defines the tilt of the polarimeter with respect to the xz reaction plane.

The measurement of one specific field component is based on the x-ray diffraction at Bragg angles θ close to 45°, where θ is defined as the angle between the incident photon and the reflecting lattice plane. From the theory of x-ray diffraction [16,17], it is known for crystals that the integrated intensity of the reflected light depends on the polarization of the incident radiation with respect to the diffraction plane via a polarization factor C. The diffraction plane is spanned here by the incident and the reflected photon. For perfect mosaic crystals we find that $C = 1$ if the electric-field vector of the incident photon is perpendicular to the diffraction plane and $C = |\cos(2\theta)|^2$ if it is parallel to the diffraction plane [17]. Therefore, at the Bragg angles θ close to 45°, the diffracted intensity is a measure of the intensity of the electric component perpendicular to the diffraction plane. By rotating the polarimeter around the z axis, the intensities $I_\sigma(\theta)$ and $I_\pi(\theta)$ are measured at the analyzer angles $\phi = 0°$ and 90°, respectively. Additionally, by changing the angle θ of the analyzer by a small amount, the x-ray fluorescence can be spectrally analyzed according to the well-known Bragg equation [18].

By using the symmetric (400) reflection of a mosaic LiF analyzer crystal, the Bragg angle amounts to 47.15° for the $L\alpha_1$ line (8398 eV) and to 47.62° for the $L\alpha_2$ (8335 eV). The contamination of the measured perpendicular field component by its parallel component, as deduced from the polarization factor, is less than 1% in both cases. The degree of linear

polarization of the $L\alpha_{1,2}$ lines, as defined by

$$P = \frac{I_\sigma - I_\pi}{I_\sigma + I_\pi}, \tag{2}$$

can be derived from the measured component intensities $I_\sigma(\theta) = I(\theta,\phi = 0^\circ)$ and $I_\pi(\theta) = I(\theta,\phi = 90^\circ)$.

For the actual implementation of the polarization measurements, we have to take into account the relatively low flux of photons that are emitted from the target after photoionization. Therefore, a relatively large area of roughly 10×15 mm^2 on the target was irradiated and the whole setup was optimized in terms of the number of detected photons and long-term stability. In order to resolve the $L\alpha$ doublet with the polarimeter, independent of the large size of the source, a Soller collimator (length of 150 mm and slit width of 0.1 mm) was mounted between the target and the analyzer crystal. The spectral broadening, as introduced by the Soller collimator, was given by a triangular divergence function with a full width at half maximum (FWHM) corresponding to $\Delta E_{\rm SC} = 7.2$ eV. Furthermore, we could benefit from an increased integrated reflectivity of a slightly mosaic lithium fluoride analyzer crystal. The reflection properties of the analyzer were measured with a double-crystal diffractometer. We observed that the width of the rocking curve was broadened by the angular distribution of the reflecting crystallites. The spectral broadening introduced by the rocking curve of the analyzer crystal was $\Delta E_C = 2.5$ eV. The diffracted photons were detected by an x-ray CCD (PI-MTE 1300B). Since the highest count rate of the detector was in just the magnitude of 5×10^{-4} photons/(s $\times$ pixel), the CCD was operated in single-photon counting mode, where the detected photons were resolved by energy. This technique enables one to discriminate unwanted events, for example, scattered radiation and fluorescence from mountings, by its energy after the data acquisition. For each angular interval $\Delta\theta$, several images were recorded with an acquisition time of 20 s. A complete spectrum for one particular angle ϕ was finished in about 24 h. The spectra were measured several times alternately at both angles $\phi = 0^\circ$ and 90°. The measured spectra kept consistent and were summed up afterward.

III. THEORY

In order to analyze the outcome of the present experiment we have also developed a theoretical approach that is based on the density-matrix theory. While the formalism presented below is for isolated atoms (or ions), the measurements are performed for the solid state. Nevertheless, it can still be applied to account for the measurements. For inner shells, such as $2p$ and $3d$ electrons of high-Z atom such as tungsten, they are tightly bounded and highly localized and thus are little affected by neighboring atoms even in the solid state. Therefore, for the $2p$ photoionization and subsequent $3d \rightarrow 2p$ radiative decay of tungsten as considered in this work, the formalism can work well, even when compared to the measurements in real experimental conditions. Within this theoretical approach, we consider the radiative decay following inner-shell photoionization as a two-step process

$$\begin{aligned} A(\alpha_i J_i) + \hbar\omega &\rightarrow A^+(\alpha_f J_f) + e^- \\ &\rightarrow A^+(\alpha_0 J_0) + \gamma + e^-, \end{aligned} \tag{3}$$

where the neutral atom A initially in its ground state $|\alpha_i J_i\rangle$ is photoionized by the incoming photon $\hbar\omega$ into the hole state $A^+(\alpha_f J_f)$. The subsequent radiative decay of the excited (hole) state to an energetically lower level $|\alpha_0 J_0\rangle$ then gives rise to characteristic x-ray emission. Theoretically, when one analyzes photon emissions from atoms or ions, the formation and subsequent decay of excited atomic levels are usually treated separately. Most conveniently, such a treatment is performed within the framework of the density-matrix theory [19,20]. In this approach, the polarization state of the excited atomic levels is described by the so-called density matrix or equivalently by the statistical tensors. Since the density-matrix description of the photoionization and subsequent radiative decay has been discussed very frequently in the past, we here restrict ourselves to a rather short account of basic formulas and refer to Refs. [21,22] for further details.

For the photoionization of atoms or ions by an unpolarized light beam that propagates along the quantization x axis as shown in Fig. 1, the statistical tensors of the photoion after photoionization are presented by

$$\begin{aligned} &\rho_{kq}(\alpha_f J_f) \\ &= \frac{\pi}{2J_i + 1}\delta_{q0} \sum_{pLp'L'} \sum_{ljJJ'} \sum_{\lambda} i^{L+p-L'-p'} \lambda^{p+p'} \\ &\quad \times [L,L',J,J']^{1/2} (-1)^{J+J'+J_f+J_i+j+1} \langle L\lambda, L' - \lambda | kq\rangle \\ &\quad \times \begin{Bmatrix} J_f & j & J' \\ J & k & J_f \end{Bmatrix} \begin{Bmatrix} J' & J_i & L' \\ L & k & J \end{Bmatrix} \langle \alpha_f J_f, \epsilon lj \\ &\quad : J \| H_\gamma(pL) \| \alpha_i J_i\rangle \langle \alpha_f J_f, \epsilon lj : J' \| H_\gamma(p'L') \| \alpha_i J_i\rangle^*, \end{aligned} \tag{4}$$

where we have assumed that the photoelectron remains unobserved. In this expression, the shorthand form $[a,b,\ldots] \equiv (2a+1)(2b+1)\cdots$ and the standard notation for the Clebsch-Gordan coefficients and the Wigner 6-j symbols have been utilized. Moreover, the reduced matrix elements $\langle \alpha_f J_f, \epsilon lj : J \| H_\gamma(pL) \| \alpha_i J_i\rangle$ describe the electron-photon interaction [23]. This interaction leads to the production of the resonance $|\alpha_f J_f\rangle$ and of the photoelectron by the photoionization of an atom in its (initial) state $|\alpha_i J_i\rangle$. Here l and j denote the orbital and total angular momenta of the photoelectron, respectively. The individual photon is characterized here in terms of the electric ($p = 1$) and magnetic ($p = 0$) multipolarities pL. In the theory of atomic collisions, the statistical tensors (4) are usually renormalized with respect to the zero-rank tensor ρ_{00} as follows:

$$\mathcal{A}_{kq}(\alpha_f J_f) = \frac{\rho_{kq}(\alpha_f J_f)}{\rho_{00}(\alpha_f J_f)}. \tag{5}$$

These reduced statistical tensors are referred to as the alignment or orientation parameters, which are independent of the particular normalization of the density matrix and are often utilized to describe the relative population of atomic sublevels $|\alpha_f J_f M_f\rangle$. Actually, the orientation and alignment

of the photoion after photoionization have been extensively investigated for many years both in theory and in experiment. For example, Kleiman and Lohmann performed a systematic theoretical study on the orientation and alignment parameters for single photoionization of atoms with the ground state $^1S_0$ by using a relaxed orbital method within a single-configurational Hartree-Fock approach [24]. For further information, refer to the reviews in [20,21,25] and references therein. In the present calculation, the photoionization field is dealt within the electric dipole $E1$ approximation, i.e., by setting $p = p' = 1$ and $L = L' = 1$ in Eq. (4). In this case, only three photoionization channels, such as $s_{1/2}$, $d_{3/2}$, and $d_{5/2}$, are allowed due to the restriction of total angular momentum and parity conservation.

After the inner-shell photoionization, the photoion appears to be in an excited state $|\alpha_f J_f\rangle$ that decays subsequently to some energetically lower state $|\alpha_0 J_0\rangle$ by the emission of a characteristic photon. In order to analyze the polarization of the characteristic photon, one has to find the photon density matrix. It is convenient to express this matrix in the so-called helicity representation, i.e., in the form $\langle \mathbf{k}_0\lambda|\hat{\rho}_\gamma|\mathbf{k}_0\lambda'\rangle$, in which $\mathbf{k}_0 \equiv (\theta_0,\varphi_0)$ and $\lambda = \pm 1$ denote the unit wave vector and helicity of the photon, respectively. The helicity part of this density matrix describes the photon polarization. If, moreover, the polarization state of the final $|\alpha_0 J_0\rangle$ level remains unobserved after the photon emission, the density matrix of the characteristic photon can be written as [22]

$$\begin{aligned}
&\langle \mathbf{k}_0\lambda|\hat{\rho}_\gamma|\mathbf{k}_0\lambda'\rangle \\
&\quad = 2\pi \sum_{kqq'} \sum_{pLp'L'} D^k_{-qq'}(\varphi_0,\theta_0,0)\rho_{kq}(\alpha_f J_f) i^{L'+p'-L-p} \\
&\qquad \times \lambda^p \lambda'^{p'} [L,L']^{1/2} (-1)^{J_0+J_f+k+q+1} \langle L\lambda, L'-\lambda'|k-q'\rangle \\
&\qquad \times \begin{Bmatrix} L & L' & k \\ J_f & J_f & J_0 \end{Bmatrix} \langle \alpha_0 J_0 \| H_\gamma(pL) \| \alpha_f J_f\rangle \\
&\qquad \times \langle \alpha_0 J_0 \| H_\gamma(p'L') \| \alpha_f J_f\rangle^*, \qquad (6)
\end{aligned}$$

where $D^k_{-qq'}(\varphi_0,\theta_0,0)$ denotes the Wigner rotation D function with its arguments φ_0, θ_0, and 0 characterized in terms of three Euler angles, which relate the propagation directions of the photoionizing and fluorescence photons by means of the corresponding three-step rotation. Moreover, the reduced matrix element $\langle \alpha_0 J_0 \| H_\gamma(pL) \| \alpha_f J_f\rangle$ represents the transition amplitude for the radiative decay $|\alpha_f J_f\rangle \to |\alpha_0 J_0\rangle + \gamma$.

To compare theoretical predictions with experimental findings, the density matrix (6) is usually parametrized in terms of the so-called Stokes parameters [19,20]

$$\langle \mathbf{k}_0\lambda|\hat{\rho}_\gamma|\mathbf{k}_0\lambda'\rangle \equiv c_{\lambda,\lambda'} = \frac{1}{2}\begin{pmatrix} 1+P_3 & -P_1+iP_2 \\ -P_1-iP_2 & 1-P_3 \end{pmatrix}, \qquad (7)$$

which are utilized to characterize the degree of both linear (P_1 and P_2) and circular (P_3) polarization of the light. The first and second lines (columns) in Eq. (7) correspond to $\lambda = +1$ and -1, respectively. The first Stokes parameter P_1 is defined to characterize the degree of linear polarization of the radiation photons relative to the x ($\phi = 0^\circ$) and y ($\phi = 90^\circ$) axes as shown in Fig. 1, which is a theoretical description of the linear polarization P from Eq. (2). The formalism of Eqs. (4)–(7) is general and thus can be applied to study the linear polarization of x-ray emissions following photoionization of any atomic ions by an unpolarized light beam. For the particular case of the inner-shell $2p_{3/2}$ photoionization of tungsten and if the $L\alpha_1$ ($3d_{5/2} \to 2p_{3/2}$) and $L\alpha_2$ ($3d_{3/2} \to 2p_{3/2}$) lines are observed perpendicular to the ionizing light, i.e., $\theta_0 = 90^\circ$ and $\phi_0 = 0^\circ$ in Eq. (6), for example, the degree of linear polarization reads

$$P_1(L\alpha_1) = \frac{3\mathcal{A}_{20}}{20-\mathcal{A}_{20}}, \qquad (8)$$

$$P_1(L\alpha_2) = -\frac{3\mathcal{A}_{20}}{\mathcal{A}_{20}+5}. \qquad (9)$$

Here $\mathcal{A}_{20}$ denotes the alignment parameter of the $2p_{3/2}$ hole state after photoionization. It is worth mentioning that Eqs. (8) and (9) have been parametrized within the $E1$ approximation of the radiation field.

As seen from Eqs. (4)–(9), any further discussion of the linear polarization has to be traced back to the computations of the bound-free transition amplitude $\langle \alpha_f J_f, \epsilon lj : J \| H_\gamma(pL) \| \alpha_i J_i\rangle$ in Eq. (4) and of the bound-bound transition one $\langle \alpha_0 J_0 \| H_\gamma(pL) \| \alpha_f J_f\rangle$ in Eq. (6). Following our previous work [21,22,26], these transition amplitudes were evaluated by using the GRASP92 [27] and RATIP [28] packages that are based on the multiconfiguration Dirac-Fock (MCDF) method [27–30]. In this method, an atomic-state wave function with parity P, total angular momentum J, and its magnetic component M is expressed as a linear combination of the configuration-state wave functions (CSFs) with the same PJM symmetry. However, in the present calculations we employed a single-configuration approximation, which was enough to obtain stable results for such an inner-shell $2p$ photoionization and subsequent $3d \to 2p$ radiative decay of tungsten. The CSFs were constructed as antisymmetrized products of a set of orthonormal orbitals and then optimized self-consistently on the basis of the Dirac-Coulomb Hamiltonian. The relativistic and QED effects were further incorporated into the expansion coefficients $c_r(\alpha)$ of the atomic states by diagonalizing the Dirac-Coulomb-Breit Hamiltonian matrix within first-order perturbation theory.

IV. RESULTS AND DISCUSSION

Figure 2 shows the polarization-resolved $L\alpha_{1,2}$ x-ray spectrum of tungsten following the photoionization of a $2p_{3/2}$ electron. The intensity of the components I_π (electric field parallel to the reaction plane) and I_σ (electric field perpendicular to the reaction plane) are measured by the polarimeter at $\phi = 90^\circ$ and $\phi = 0^\circ$, respectively. From a comparison of the peak intensities at the two field directions one can readily recognize the essential feature of our measurements. For the $L\alpha_1$ line, the I_σ component is stronger than the I_π component, whereas it is the opposite for the $L\alpha_2$ line. From the measurement it is obvious that the two emitted spectral lines are (linearly) polarized to some degree but the sign of the polarization is reversed.

In order to analyze the degree of polarization, we performed a detailed analysis of the measured line profile. For the present spectrometer the signal $I_{\sigma,\pi}(\theta)$ at the detector can be described in a simplified manner as a convolution of the spectral intensity distribution of the source, the divergence function of the collimator geometry, and the rocking curve of the crystal. For those distributions the angular and spectral

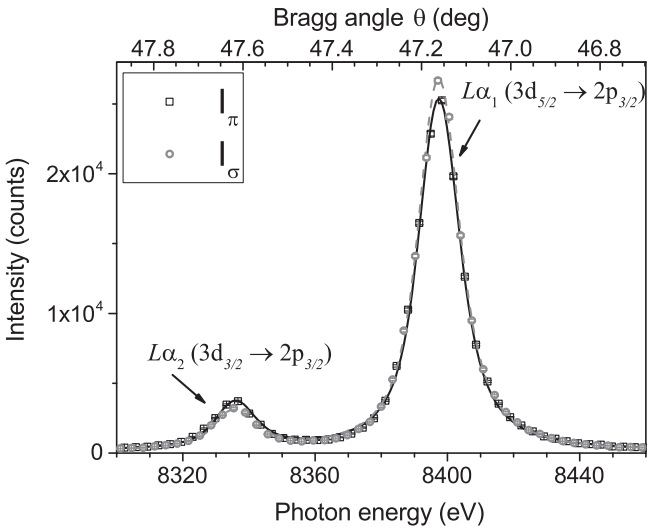

FIG. 2. Measured $L\alpha_1$ and $L\alpha_2$ intensity for the two analyzer angles $\phi = 90°$ [$I_\pi(\theta)$, black squares] and $\phi = 0°$ [$I_\sigma(\theta)$, gray circles]. These intensities refer to the electric field parallel π and perpendicular σ to the reaction plane. In addition, the error bars are plotted for each data point. The ratio of the emitted intensities $I(L\alpha_1)/I(L\alpha_2)$ is clearly dependent on the direction of the electric-field component, showing the alignment of the excited ionic (hole) state following the photoionization. The plotted lines represent a fit to the measured data as described in Sec. IV.

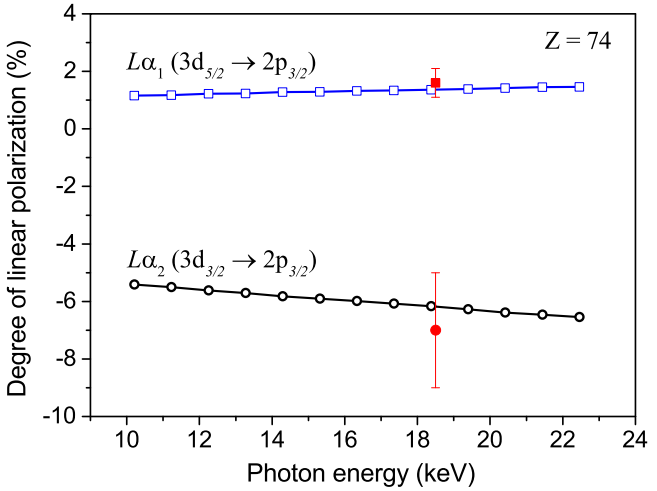

FIG. 3. Degree of linear polarization of the $L\alpha_1$ ($3d_{5/2} \rightarrow 2p_{3/2}$, blue open squares) and $L\alpha_2$ ($3d_{3/2} \rightarrow 2p_{3/2}$, black open circles) emission following the inner-shell $2p_{3/2}$ photoionization of tungsten atoms by an unpolarized photon beam as a function of the ionizing photon energy. Calculations performed within the MCDF method are compared with the experimental measurements (red closed circles).

arguments are related by the dispersion relation determined by the derivation of the Bragg equation [18]. The plotted lines in Fig. 2 present this convolution assuming two Lorentzian functions (with FWHMs of 7.8 and 7.4 eV [31]) for the L-line shapes, a triangle divergence function for the Soller collimator, and the measured rocking curve of the LiF crystal. The only fit parameters of the measured intensities $I_\sigma(\theta)$ and $I_\pi(\theta)$ are the intensities of the two L lines. As can be clearly seen from Fig. 2, this fitting reproduces the measured data very well over the whole spectral range. The measured linewidth is in accord with the spectral broadening due to the collimator function and the rocking curve. The energy splitting of the $L\alpha$ doublet and the overall line shape do not change significantly for the σ and π components. From the fitted intensities of the Lorentzian spectral lines and by using Eq. (2), the degree of linear polarization is determined as $P(L\alpha_1) = +(1.6 \pm 0.5)\%$ and $P(L\alpha_2) = -(7 \pm 2)\%$, respectively.

In Fig. 3 we compare the theoretical results with the experimental findings. The degree of linear polarization of the $L\alpha_{1,2}$ lines following the ionization of a $2p_{3/2}$ electron of tungsten by an unpolarized photon beam has been calculated within the MCDF method, which is plotted as a function of the ionizing photon energy in the range of 10–23 keV. The theoretical calculation shows a weak dependence of the degree of linear polarization on the ionizing photon energy for both lines. For the $L\alpha_1$ line, the most intense line of the L-shell emission, the calculated polarization is positive with very small values between 1% and 2%. In contrast, for the $L\alpha_2$ line the calculated polarization is negative with values between -5% and -7%. The experimentally observed data, plotted in red in Fig. 3 at the average photon energy $\bar{E}$ of 18.5 keV, are in very good agreement with the calculations. Due to the only weak dependence of the calculated polarization of the $L\alpha_{1,2}$ lines on the photon energy, the correspondence between theory and the experimental results is not affected much by the nonmonochromatic effect of the photoionizing radiation.

On the other hand, we want to stress that the use of a crystal-based analyzer is essential for a successful polarization measurement, as the $L\alpha$ doublet is typically not resolved by solid-state detectors. The linear polarization of such an unresolved superposition of two spectral lines is marginal due to the mutual cancellation of the polarizations of the $L\alpha_1$ and $L\alpha_2$ components.

It is worth mentioning that the ratio $I(L\alpha_1)/I(L\alpha_2)$, which is known with high accuracy because it can be measured very easily with x-ray spectrometers, actually depends on the direction of the measured electric-field component. In the present experiment, this intensity ratio is determined as 0.108 ± 0.01 for the σ component and 0.127 ± 0.01 for the π component. From the measured intensity ratios, a polarization-averaged ratio 0.118 ± 0.01 is determined, which is in good agreement with the available value 0.114 ± 0.002 in Ref. [31] and references therein.

Finally, the alignment parameters $\mathcal{A}_{20}(L\alpha_1) = 0.11 \pm 0.07$ and $\mathcal{A}_{20}(L\alpha_2) = 0.12 \pm 0.07$ can be deduced from the measured degree of linear polarization by using Eqs. (8) and (9), respectively.

V. CONCLUSION

In this work we have shown by means of a well characterized x-ray polarimeter that the L-shell fluorescence lines $L\alpha_1$ and $L\alpha_2$ of tungsten are partially polarized. The measurement could be confirmed within the experimental errors by a theoretical simulation of the photoionization and subsequent radiative decay based on the density-matrix theory. This work shows that the combination of crystal-based x-ray spectropolarimetry, combined with highly sophisticated

atomic physics simulation, could be the basis for reliable investigations of atomic alignment of atoms after defined excitation by photon or particle beams. The use of brilliant x-ray sources such as synchrotrons of third generation or x-ray free-electron laser beams could improve such investigations by orders of magnitude and allow one to study atoms in a much more defined circumstance compared to the present work. Such potential applications of this technique could help us further explore new insights to atomic (or matter) structure.

ACKNOWLEDGMENTS

This work was supported by the Deutsche Forschungsgemeinschaft (Germany) and the Bundesministerium für Bildung und Forschung (Germany). Z.W.W acknowledges support from the Helmholtz Institute Jena (Germany) and the Research School of Advanced Photon Science of Germany and also from the National Natural Science Foundation of China (China) under Grant No. 11464042.

[1] W. Mehlhorn, Phys. Lett. **26A**, 166 (1968).
[2] S. Flügge, W. Mehlhorn, and V. Schmidt, Phys. Rev. Lett. **29**, 7 (1972); **29**, 1288(E) (1972).
[3] S. C. McFarlane, J. Phys. B **5**, 1906 (1972).
[4] J. H. Scofield, Phys. Rev. A **14**, 1418 (1976).
[5] E. G. Berezhko, N. M. Kabachnik, and V. M. Rostovsky, J. Phys. B **11**, 1749 (1978).
[6] Z. W. Wu, J. Jiang, and C. Z. Dong, Phys. Rev. A **84**, 032713 (2011).
[7] Z. W. Wu, C. Z. Dong, and J. Jiang, Phys. Rev. A **86**, 022712 (2012).
[8] C. D. Caldwell and R. N. Zare, Phys. Rev. A **16**, 255 (1977).
[9] W. Sandner and W. Schmitt, J. Phys. B **11**, 1833 (1978).
[10] H. Yamaoka, M. Oura, K. Takahiro, N. Takeshima, K. Kawatsura, M. Mizumaki, U. Kleiman, N. M. Kabachnik, and T. Mukoyama, Phys. Rev. A **65**, 062713 (2002).
[11] I. Han, Angular Dependence of Fluorescence X-Rays and Alignment of Vacancy State Induced by Radioisotopes, edited by N. Singh (InTech, 2011), available at http://www.intechopen.com/books/radioisotopes-applications-in-physical-sciences/angular-dependence-of-fluorescence-x-rays-and-alignment-of-vacancy-state-induced-by-radioisotopes.
[12] H. Küst, U. Kleiman, and W. Mehlhorn, J. Phys. B **36**, 2073 (2003).
[13] H. Yamaoka, M. Oura, K. Takahiro, K. Kawatsura, S. Ito, M. Mizumaki, O. Oohashi, Y. Ito, and T. Mukoyama, J. Phys. B **39**, 2747 (2006).
[14] R. A. Barrea, C. A. Pérez, T. S. Plivelicl, E. V. Bonzi, and H. J. Sánchez, J. Phys. B **38**, 839 (2005).
[15] For the measurements, a 125-μm-thick tungsten XRF spectroscopic standard target from Micro-Analysis Consultants Ltd. was used.
[16] A. Authier, *Dynamical Theory of X-Ray Diffraction* (Oxford University Press, New York, 2004).
[17] W. H. Zachariasen, *Theory of X-Ray Diffraction in Crystals* (Dover, New York, 1945).
[18] B. G. Agarwal, *X-Ray Spectroscopy* (Springer, Berlin, 1991).
[19] K. Blum, *Density Matrix Theory and Applications* (Plenum, New York, 1981).
[20] V. V. Balashov, A. N. Grum-Grzhimailo, and N. M. Kabachnik, *Polarization and Correlation Phenomena in Atomic Collisions* (Kluwer Academic, New York, 2000).
[21] N. M. Kabachnik, S. Fritzsche, A. N. Grum-Grzhimailo, M. Meyer, and K. Ueda, Phys. Rep. **451**, 155 (2007).
[22] L. Sharma, A. Surzhykov, M. K. Inal, and S. Fritzsche, Phys. Rev. A **81**, 023419 (2010).
[23] S. Fritzsche, A. Surzhykov, and T. Stöhlker, Phys. Rev. A **72**, 012704 (2005).
[24] U. Kleiman and B. Lohmann, J. Electron Spectrosc. Relat. Phenom. **131-132**, 29 (2003).
[25] H. Kleinpoppen, B. Lohmann, and A. N. Grum-Grzhimailo, *Perfect/Complete Scattering Experiments: Probing Quantum Mechanics on Atomic and Molecular Collisions and Coincidences* (Springer, Berlin, 2013).
[26] Z. W. Wu, N. M. Kabachnik, A. Surzhykov, C. Z. Dong, and S. Fritzsche, Phys. Rev. A **90**, 052515 (2014).
[27] F. A. Parpia, C. F. Fischer, and I. P. Grant, Comput. Phys. Commun. **94**, 249 (1996).
[28] S. Fritzsche, Comput. Phys. Commun. **183**, 1525 (2012).
[29] S. Fritzsche, J. Electron Spectrosc. Relat. Phenom. **114-116**, 1155 (2001).
[30] I. P. Grant, *Relativistic Quantum Theory of Atoms and Molecules* (Springer, New York, 2007).
[31] R. Diamant, S. Huotari, K. Hämäläinen, R. Sharon, C. C. Kao, and M. Deutsch, Phys. Rev. A **63**, 022508 (2001).